Proceedings World Geothermal Congress 2015
Melbourne, Australia, 19-25 April 2015

Characterisation of Natural Fractures and Fracture Zones of the Basel EGS Reservoir Inferred from Geophysical Logging of the Basel-1 Well

Martin Ziegler, Benoît Valley and Keith F. Evans

Department of Earth Sciences, ETH Zurich, Sonneggstrasse 5, 8092 Zurich, Switzerland

corresponding author: martin.ziegler@erdw.ethz.ch

Keywords: geothermal energy; acoustic televiewer data; stick-slip correction; fracture set characteristics.

ABSTRACT

The development of a geological model for the reservoir of an Enhanced Geothermal System (EGS) provides an essential framework for geomechanical models that simulate reservoir behaviour during the stimulation and production phases. The geological model describes the spatial distribution and scaling of discontinuities within the reservoir as well as lithological variations. In this paper we analyse logging data from the 5 km deep well, Basel-1, located in Switzerland to investigate the natural fractures and zones characterised by high fracture frequency in the crystalline basement. The logs extend from 2.6 km depth, about 100 m below the weathered palaeo-surface of the granite, to a depth of 5.0 km, and include acoustic televiewer (UBI), density and p-wave velocity. The results of drill cuttings analysis were also available. Two previous analyses of the UBI log have been made. Considerable differences in the distributions of natural fractures in the crystalline basement were found from the three analyses. The differences in large part reflect the difficulty in distinguishing natural from drilling-induced fractures. Poor quality images in the open-hole section below 4.7 km resulting from stick-slip motion of the UBI sonde were radically improved by applying a novel correction method using accelerometer data. This led to fewer natural fractures in the open section than recognised in earlier studies. Fracture frequency decreases with depth from 3.1 fractures/m near the top of the logged section to 0.3 fractures/m below 3.0 km. Orientation cluster analyses revealed a complex pattern of up to 6 potential fracture sets along the well, some of which may be conjugate pairs. Only set 1 (steeply dipping to W–SW) is present along the entire imaged borehole, the other sets occurring over limited sections of the hole. The mean orientation of set 1 does not coincide with prominent NNE-striking Rhenish lineaments (faults) of first- and second-order in the Basel area, but strikes subparallel to the maximum principal horizontal stress. Fractures belonging to set 1 are spatially clustered and form localised zones of high fracture frequency. Zone lengths ranged up to 100 m, but were more typically tens of metres, and below 4.0 km the zones consisted predominantly of fractures belonging to set 1. Zones of high fracture frequency did not necessarily coincide with low density or low p-wave velocity anomalies, as might be expected from fracture zones with damage or higher porosity.

1. INTRODUCTION

An essential step towards developing a petrothermal reservoir is to characterise the lithology and structural discontinuities within the target rock mass to produce a *geological model* of the reservoir. The structural discontinuities we distinguish are: single fractures of dimensions up to tens of metres; fracture zones of length up to a kilometre that are composed of clusters of smaller-scale fractures; and faults at larger scale. Geological models provide the essential framework for *geomechanical models* that are used to simulate the changes in rock mass permeability resulting from stimulation operations or later production phases. Such changes are primarily governed by the characteristics of the pre-existing fracture population, and its relationship to the in-situ stress state. This is especially true for crystalline formations characterised by a low-permeability matrix. Discontinuity data are typically derived from geophysical logs run in one or more boreholes that intersect the reservoir. This information provides essentially scanlines, usually vertical, through the penetrated structures. Further information about the structures remote from the wellbores can come from geophysical methods such as vertical seismic profiles (VSP), or detailed analysis of the spatial patterns of microseismicity generated during the stimulation operations. However, the available information is usually sparse, and the development of geological models is challenging. This is the case for the rock mass targeted in the Basel Deep Heat Mining (DHM) project, where the primary source of discontinuity data in the granitic reservoir stems from logs run in the Basel-1 borehole, which was drilled to 5 km depth between May and October 2006 as the first hole of a duplet. The hole entered intact granite at 2507 m below ground (Ladner et al., 2008). An earlier reconnaissance borehole, Otterbach-2, drilled to 2755 m depth in 2001 at a location 1 km southeast of Basel-1 entered granite at 2649 m below ground (Häring, 2001). The lowermost 371 m of Basel-1 was subjected to a large, high-pressure stimulation injection in December 2006 to attempt to increase the permeability of the rock mass and create a heat exchanger. The injection was terminated after an earthquake with magnitude exceeding M_L 3 was registered, the largest event of M_L 3.4 occurring shortly after shutting-in the well (Deichmann et al., 2014, and references therein). These led to cessation of the DHM project and to extensive geomechanical investigations of the causes of such unexpectedly large events. In this paper we describe natural discontinuities along the borehole as the first step towards developing a geological model of the stimulated rock mass.

The Basel-1 borehole is approximately vertical and reaches a depth of 5009 m below the rotary table of the rig, which is 9 m above ground level and 259.2 m above sea level. All depths in Basel-1 given in this article are measured along hole from the rotary table unless stated otherwise. The borehole is completed with 7-5/8 inch liner with the shoe set at 4638 m (details are given in Häring et al. (2008) and Valley and Evans (2009)). Prior to installing this casing, a suite of borehole logs was run from hole bottom to the 10-3/4 inch liner shoe at 2602 m, which is 182 m below the granite top. The hole size in this section is 9-7/8 inch to 4841 m, and 8-1/2 inch below. The logs run included: ultrasonic televiewer (UBI), 2-arm caliper, spectral gamma ray, sonic (s- and p-wave velocities), density, and temperature.

Two independent studies of the fractures imaged in the UBI log have already been published. These show considerable differences in the total counts of features recognised as natural fractures (rather than drilling-induced fractures): the study reported by Häring et

al. (2008) identified 983 natural fractures whereas that of Fabbri (2011) found 1461. The relative fractions of fractures identified as high and low confidence also differed over many borehole intervals. These differences largely reflect the difficulty of distinguishing between pre-existing and drilling-induced fractures, which is particularly acute for Basel-1 UBI log. Moreover, image quality below 4677 m is poor owing to the occurrence of stick-slip movement of the sonde. Häring et al. (2008) identified two major 'cataclastic fracture zones' in the open-hole section which intersected the well over several metres at ~4700 and ~4835 m depth. In addition, two localised zones of higher fracture frequency were found at ~4670–4680 and ~4760–4775 m (Ladner, 2014, pers. comm.). However, few details of these zones were reported, and potential fracture zones above the open borehole section of the well were not investigated in detail. Käser et al. (2007) examined drill cuttings and found several localised zones along the well which showed evidence of argillic alteration and occasionally contained anhydrite, which they interpreted to indicate cataclastic zones (i.e., zones formed of cohesive, brittle fault rock; for nomenclature see, e.g., Heitzmann (1985); cf., Meyer (1987)). Fracture zones are taken here to refer to discontinuity structures of lengths tens of metres to a kilometre that consist of a quasi-planar connected network of single fractures having lengths up to tens of metres (Valley, 2007). Fracture zones, by virtue of their length, are usually hydraulically-significant structures, and are believed to exert a considerable influence on the response of the rock mass to stimulation injections (Evans et al., 2005). Length, orientation, width, internal structure and spacing are key attributes of fracture zones that we would like to better understand. In this article we will focus on the last four points, since the length of fracture zones cannot simply be inferred from a single borehole dataset. Our goals of this study are to re-analyse the occurrence of natural fractures, to identify fracture sets and their spacing statistics, to determine in detail the structural characteristics and locations of zones of high fracture frequency, and to supplement the acoustic reflectivity information with data from additional logs.

2. GEOLOGICAL SETTING

2.1 Geotectonic Overview

The city of Basel is located at the southeastern margin of the Upper Rhine Graben (URG) north of the fold and thrust belt of the Jura Mountains in northwestern Switzerland (Figure 1a). The URG is the southern part of the Rhine Graben that reaches from about the city of Mainz in Germany to Basel, and is one of the most prominent structures of the European Cenozoic rift system that extends from the North Sea to the Mediterranean (Ziegler, 1992). Distinct episodes in URG rifting (late Eocene activation, Oligocene main rifting, and early Miocene inactivation of the extension of Rhône Valley and Massif Central grabens) can be linked to distinct periods of Alpine deformation (Laubscher, 2001; Dèzes et al., 2004). The subsurface of the southern part of the URG consists (from W to E) of the Dannemarie Basin and several 'tilted blocks' of a few 100 km^2 in size (Altkirch, Sierenz, Basel, and Dinkelberg Block, which collectively form the so-called *'Tilted Block Array'*) that are delimited by steep NNE-striking fault zones ("Rhenish" first-order faults; Gürler et al., 1987, and references therein; Hinsken et al., 2007: Fig. 2). The km-scale faults cut across the Mesozoic and Cenozoic cover rocks of 2–3 km thickness as well as the Palaeozoic basement. Internal, second-order faults of the Basel Block strike NNE-SSW (parallel to first-order faults), NW-SE (Hercynian), and ~W-E (associated with Permian-Carboniferous troughs) (Gürler et al., 1987; Ustaszewski, 2004). Reactivation of a NNE-striking fault ("Rhenish fault"), which parallels the major faults of the URG, or of a WNW-ESE-trending basement fault belonging to the ENE-striking Rhine-Bresse Transfer Zone are thought to be the most likely candidates to have caused the disastrous 1356 Basel earthquake (Ustaszewski and Schmid, 2007).

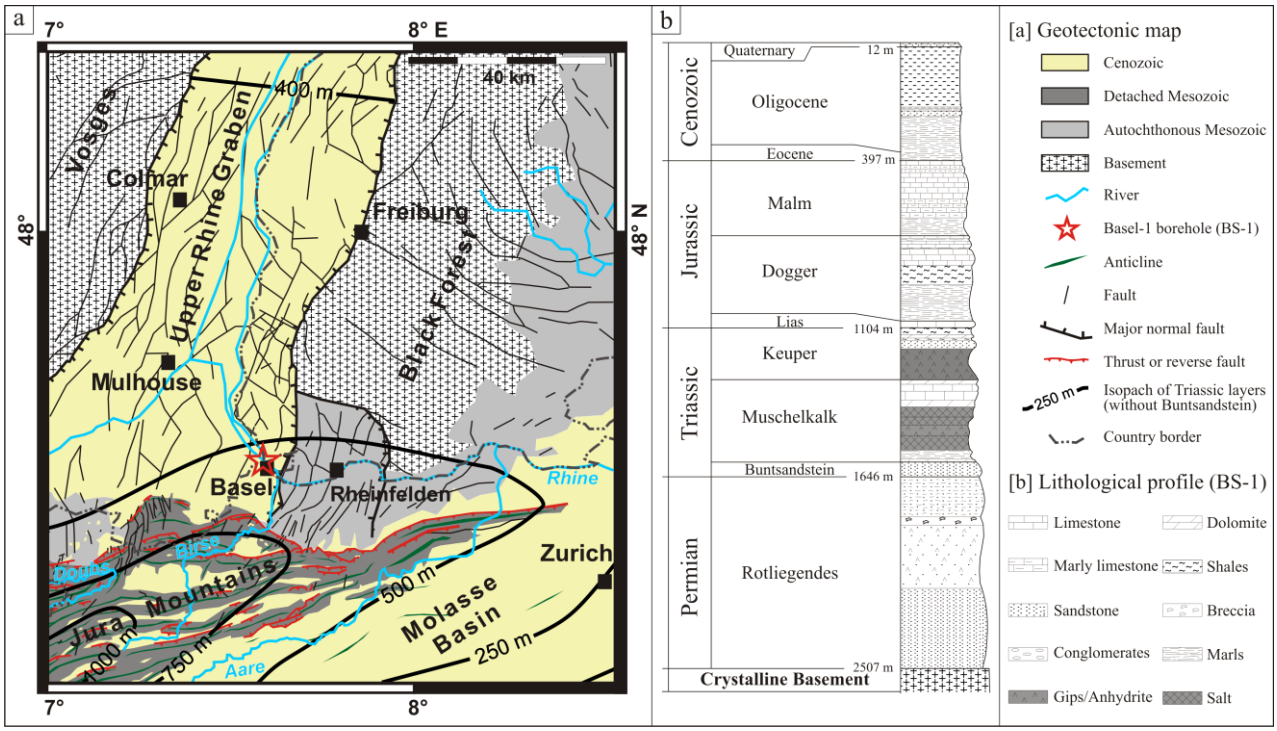

Figure 1: (a) Geological structures around Basel. (b) Lithological sequence along the Basel-1 borehole (modified after Valley and Evans (2009); formation depths measured from ground surface after Ladner et al. (2008)).

2.2 Lithological Sequence along the Basel-1 Borehole

The lithological profile along the Basel-1 borehole was determined primarily from analysis of drill cuttings. A core sample taken from 4909 to 4917 m was available for thin section analysis. The core sample contained no natural fractures. The crystalline basement is overlain by Quaternary, Cenozoic, Mesozoic (Jurassic and Triassic), and Permian sedimentary rocks with a collective thickness of 2507 m (Figure 1b). The borehole section between 2411 and 2507 m below ground surface consists of a 'transition zone' containing Rotliegend siltstones and crystalline rocks. The crystalline basement is mainly composed of granitic rocks, and to a minor extent, of lamprophyric and aplitic dykes. The compositions of the granitic rocks range from hornblende-bearing, quartz-rich biotite-granites (coarser-grained) at the top of the basement to monzogranites and monzonites with decreased contents of quartz (finer-grained) at deeper borehole sections (Käser et al., 2007). The core sample contains monzogranites and monzonites with an isotropic to fluidal texture (i.e., oriented potassium feldspar phenocrysts and elongated clusters composed of hornblende and biotite). Geochemical analysis suggests that the granitic rocks are of I-type (i.e., igneous magma origin), in contrast to the S-type granites (i.e., magma originating from partial melting of sedimentary source rocks) typically found in the southern Black Forest (Käser et al., 2007). The granitic rocks show different types of high- and low-temperature hydrothermal alteration, such as the formation of Ca-Al-silicates (e.g., albite, epidote), anhydrite, calcite, and clay minerals (illite-muscovite and mixed layer smectite-illite). Käser et al. (2007) found several zones of argillic alteration and anhydrite, which they associated with cataclastic (brittle shear) fracturing. The most prominent such zone extended between 4830.2 and 4835.6 m (see Section 4.4).

3. LOG DATA AND ANALYSIS METHOD

3.1 Log Data and Data Processing

Borehole logs were run in the crystalline section of Basel-1 shortly after completion of drilling operations when the hole was open from the 10-3/4 inch liner shoe at 2602 m to hole bottom. The logs are listed in Table 1, and were run by Weatherford on 23rd October and Schlumberger on 27th and 28th October 2006. The depth scale of the Weatherford logs was used as the reference. The Schlumberger logs were depth-matched to the depth scale of the Weatherford logs using the natural gamma logs. All logs were sampled at 12.5 cm except for the UBI, which was 1 cm for the image logs and 15 cm for the natural gamma ray.

Table 1: Borehole sondes and data used

Weatherford	Schlumberger
Total Gamma Ray (TGR)	Total Gamma Ray (TGR)
Spectral Gamma Ray (SGR)	Ultrasonic Borehole Imager (UBI)
Monopole-Dipole Array (MDA)	Caliper from UBI (CSA)
Spectral P_e density (SPeD)	
2-arm caliper (Kal)	

Logs of rock mass bulk density, ρ_b, p-wave velocity, v_P, and s-wave velocity, v_S, were provided by Weatherford. The velocity (MDA) and density (SPeD) logs were combined to obtain profiles of the dynamic elastic properties of the rock surrounding the borehole. The Spectral Gamma Ray (SGR) data was processed by Weatherford to give fractional abundances of potassium, thorium, and uranium, which is useful for identifying petrographic changes along the borehole.

The Schlumberger Ultrasonic Borehole Imager (UBI) measures the acoustic reflectivity of the borehole wall (amplitude log) and the two-way travel time of the ultrasonic pulse to the borehole wall (travel time log). There were 180 pulses per revolution of the transponder, and swathes were 1 cm apart. Further details of the log are given in Valley and Evans (2009). Fluid velocity in the borehole was also measured so that the travel-time log could be converted into a borehole geometry log, from which a cross-sectional area log (CSA) could be derived. Single-point outliers (i.e., spikes) in the CSA log were removed by interpolation between adjacent data points. The maximum borehole diameter inferred from the UBI travel time log conformed to the diameter from the mechanical caliper (Kal), indicating that the UBI travel time log was not affected by the 'time-out' set by the data acquisition system for registration of the return pulse. The UBI tool was run centralised with a logging speed of 4 m/min up the borehole from 5000.5 m to the top of the 10-3/4" liner shoe at 2602 m. The orientation of the UBI log is disturbed by the metal of the liner down to about 2609 m. Below 4677 m the UBI data is almost continuously affected by stick-slip motion of the tool. The combination of elasticity in the logging system and frictional resistance between the tool centralisers and the borehole wall generates irregular tool motion in the form of an alternation of stops and sudden acceleration. Such irregular motion of the tool is absorbed by the elasticity of the wireline and is not detected by the depth encoding device located on surface. This leads to a cyclical distortion of the depth scale of the acquired image, where periods when the sonde is stuck and the same part of the borehole is repeatedly scanned alternate with periods of tool acceleration/deceleration, where the scanned swath corkscrews up the hole to the next stationary depth. An example of the image is shown in Figure 2a. On the raw log, the stationary periods extend mostly for 10–30 cm (with a mean of 21 cm), and the periods of acceleration/deceleration are mostly 20–40 cm long. More than 500 'stick-slip' cycles were identified below 4677 m. The stick-slip motion makes the identification and dip determination of discontinuities difficult at best. To overcome this problem, the images were corrected for the stick-slip motion using the records from the vertical accelerometer of the UBI orientation tool (GPIT). The correction was applied by first removing the gravity component from the net acceleration record using tool inclination to obtain the motion component of the tool's acceleration. This was then integrated twice with respect to time to give the estimated displacement. An example of the corrected amplitude image is shown in Figure 2b.

An additional difficulty for identifying natural fractures came from the fact that about 81% (1954 m) of the log is affected by stress-induced breakouts whose direction is sub-normal to the strike of a prominent natural fracture set (Valley and Evans, 2009). Thus, the high and low points of these fractures lie within the breakout failure sector, which occasionally made the fitting of a sinusoid to the unwrapped image less certain. Furthermore, the occurrence of drilling-induced fractures of unknown origin (DIF) that also strike sub-perpendicular to the breakouts (Figure 2b; cf., Sikaneta and Evans, 2012) made natural fracture identification difficult in places.

3.2 Analysis Method

3.2.1 Natural Fractures

The location and orientation of natural fractures were analysed by fitting sinusoidal curves to visible traces in the unwrapped UBI acoustic reflectivity log using WellCAD software by Advanced Logic Technology. Fracture orientation was corrected for non-vertical borehole direction (the borehole deviates by up to 8° from vertical). Our analysis assumed a cylindrical borehole and, thus, neglected the effect on fracture dip angles of non-circular borehole geometry caused by borehole breakouts. This effect was analysed by Fabbri (2011). Comparison of apparent dip angles of random fractures from Fabbri (2011) with our results, however, revealed that the differences in dip angles caused by non-cylindrical borehole geometry was always less than 3°.

An important aspect of the analysis was to distinguish natural fractures from fractures induced by the drilling process. Examples of the latter are indicated in Figure 2 and include axial (A-DITF; Figure 2c) and en-echelon (E-DITF; Figure 2d) drilling-induced tensile fractures, and drilling-induced fractures of unknown origin (DIF; Figure 2b). In contrast to drilling-induced fractures, natural fractures are not geometrically related to the borehole and commonly occur as full sinusoidal traces along the borehole wall. Such full-trace sinusoidal features were denoted as *'certain'* natural fractures. Fractures that terminated against certain natural fractures and thus did not have full sinusoidal traces were not recognised as certain. Drilling-induced fracture traces occur at specific locations around the borehole wall, such as parallel to the borehole axis in case of A-DITFs (Figure 2c; see review by Schmitt et al. (2012)), and can show further characteristics, such as regular spacing compared with natural fractures. An example is shown by the clusters of E-DITFs evident in Figure 2d (e.g., Valley, 2007). Clusters of steeply-dipping, closely-spaced (~0.1–0.3 m) natural fractures have not been observed in analogue outcrops of crystalline rocks. Features that could not be clearly identified as either a natural or drilling-induced fractures were classified as *'uncertain'*, meaning that they were considered as potential natural fractures.

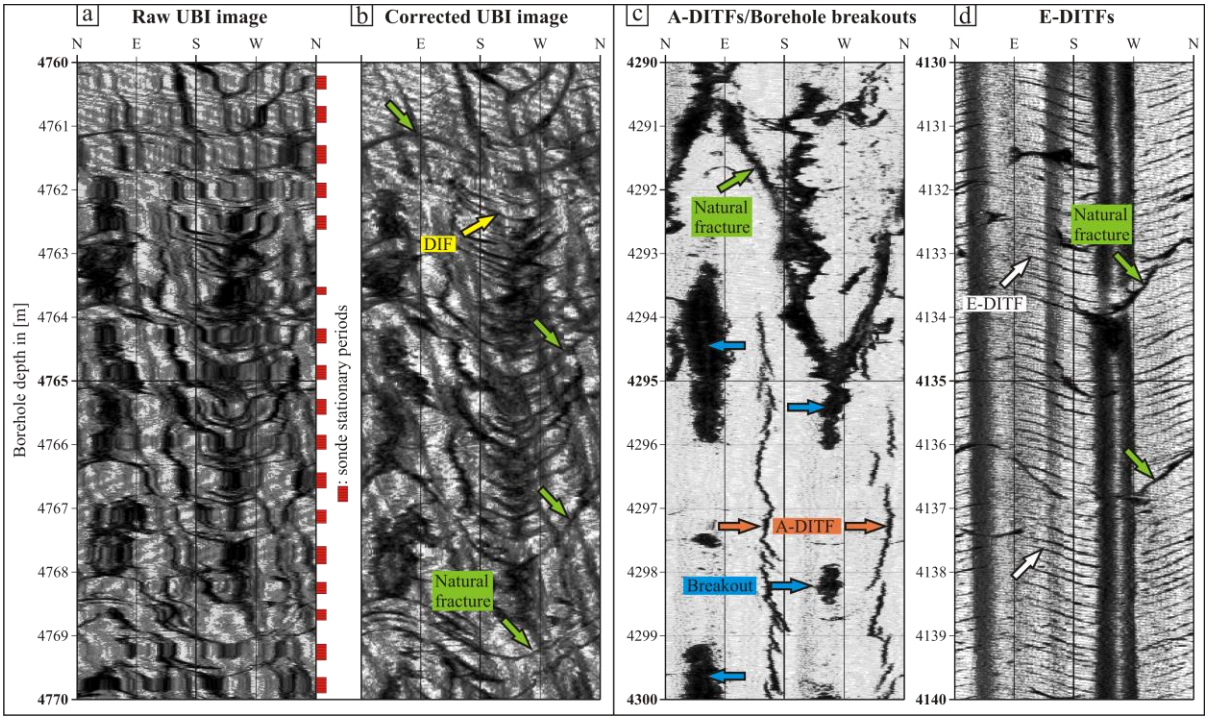

Figure 2: (a) Raw image affected by cyclic stick-slip motion of the sonde leading to image distortion. (b) The same log after correction. (c) Section where both axial DITFs and breakouts occur — the A-DITFs are ~90° offset from breakouts. (d) E-DITFs with regular fracture spacing of about 0.1–0.3 m. Green arrow: natural fracture; orange arrow: A-DITF; white arrow: E-DITF; yellow arrow: DIF; blue arrow: breakout; background: UBI amplitude image.

Fracture set identification and analysis was carried out for twelve non-overlapping 200 m intervals, denoted I to XII, between 2600 and 5000 m utilising fuzzy (orientation) cluster analysis (Hammah and Curran, 1998). Both certain and uncertain natural fractures were included. Seed points for fuzzy cluster analysis were manually chosen based on fracture pole density plots, and a constant cluster search radius of 25° was used to account for the possibility that the orientation of a fracture set changes within the 200-m-intervals. Fracture orientation clusters with less than 5 fractures for the interval in question were excluded from further analysis (denoted as *rest* in Table 2). Cluster mean orientation was calculated considering the bias introduced by unequal angular differences between the fractures of a set and the borehole trajectory (Terzaghi, 1965; Priest, 1993). We used a minimum bias angle of 15° to avoid skewing of weighted data. The results of the cluster analysis yielded a number of distinct fracture sets for each 200 m interval. The mean value of fracture set spacing was calculated for each set in each 200 m borehole interval. We used the mean orientation of each fracture set to calculate an estimate of 'true' from apparent spacing for the set in question. Fracture sets with considerably smaller true spacing compared to other fracture sets within the same borehole interval are called *dominant* set(s) in this article.

3.2.2 Fracture Frequency and Fracture Zones

The cumulative count of all fractures (certain and uncertain) along the well is shown in Figure 3. The implied average fracture frequency decreases with depth, and is 3.1 fracture/m in the uppermost depth range 2.6–2.65 km, 1.3 fractures/m in the range 2.65–3.0 km, and 0.3 fractures/m below 3.0 km. Localised zones of higher fracture frequency may indicate fracture zones that cut the

well, although other explanations are possible. We note also that fracture zones intersecting the well do not necessarily have a high fracture frequency since the borehole may penetrate the zone at a location where only few fractures are present. Nevertheless, to identify potential fracture zones, we analysed fracture frequency along the well in averaging intervals of 2 and 10 m length. Prior to this, we removed trends of 2.8 fractures/m and 1.0 fractures/m, respectively, from the fracture frequency profile in the upper two intervals (2.6–2.65 km and 2.65–3.0 km) to reduce the profile to a uniform background frequency of 0.3 fractures/m. Any negative values in the residual were set to zero. For the 10 m averaging length applied to the residual, intervals were considered to host a high frequency of fractures if the residual fracture frequency was ≥ 0.5 fractures/m. Adjacent intervals of high fracture frequency were joined into a single zone, and all zones denoted as FZ-10m. Moreover, intervals immediately adjacent to such zones were also included in the zone if their residual fracture frequency was ≥ 0.25 fractures/m. To facilitate comparison with anomalous zones in the density and velocity profiles, which were often narrower than 10 m, a similar procedure to identify zones of high fracture frequency was conducted using 2 m intervals. In this case, the threshold residual frequency for the shorter interval was taken as ≥ 1 fracture/m, but only provided that the resulting zone length was > 4 m. If the resulting zone length was 4 m or less, the threshold was increased to ≥ 3 fractures/m. This excluded short zones with only moderately high fracture frequency. Again adjacent intervals with ≥ 0.5 fractures/m were included in the zone. The resulting zones of high fracture frequency were denoted as FZ-2m.

The damage and porosity accrued through the development of a fracture zone may result in a lower density and lower p-wave velocity within the zone. Thus, we made a first attempt to detect zones characterised by anomalously low density (LDZ) and low velocity (LVZ) by visually identifying negative excursions in the density and/or velocity profiles below the local background fluctuations. We recognised that this provisional procedure may not have identified all low density/velocity zones.

4. RESULTS

4.1 Analysis of Fracture Sets

Figure 4 presents stereographic plots of poles to all fractures (certain and uncertain) for each 200 m depth interval (denoted as intervals I–XII in Figure 4). The poles to all fractures in all intervals (i.e., between 2600 and 5000 m) are shown as interval XIII-a. Distinct clusters of poles are evident in some plots (e.g., interval V) whereas others show greater scatter (e.g., intervals VII and IX), indicating that the mean orientations of fracture clusters within the intervals change along the borehole, as noted by Ladner et al. (2008). Six probable fracture sets were identified from the analysis, all with essentially steep (45–75°) or very steep (> 75°) mean dip angles. The mean orientation and total number of fractures defining each set in each interval are listed in Table 2. Each interval contains between 1 and 5 of the 6 recognised fracture sets, indicating discontinuous occurrence of some of the sets along the hole. Figure 3 presents the repartition of fracture sets versus depth. Set 1 (WSW-dip/steep) and set 2 (ENE-dip/steep) host most fractures and constitute the dominant sets, in agreement with results from Ladner et al. (2008) and Fabbri (2011). Fractures of set 1 occur in all intervals, but members of set 2 are largely restricted to 2600–3200 m, and occur only sporadically below 3200 m. The majority of the fractures identified in the lowermost ~600 m of the borehole, which includes the open-hole section below 4638 m, belong to set 1, and are mostly denoted as uncertain rather than certain natural fractures, even after processing the images to reduce the effects of stick-slip movement of the sonde. Set 3 (S–SSW-dip/steep to very steep) fractures are limited to ~2600–2900 m and 4000–4300 m. Fractures of set 4 (WNW–NW/steep to very steep) are limited to 2800–4200 m and are dominant between ~3000 and 3600 m. Set 5 (NNE–NE-dip/steep) is of minor importance. Fractures assigned to set 6 (ESE–SE-dip/very steep) are rare, and could either be conjugate or belong to set 4.

The 'true' mean spacing between fractures in each set for each interval is listed in Table 3. The mean fracture spacing ranges from 0.6 m to 17.2 m considering all sets. The dominant sets (i.e., those with the smallest fracture spacing; see Section 3.2.1) have a mean spacing of: 0.6 m in interval I (set 2); 0.9 m and 1.2 m in interval II (sets 1 and 2); and 1.6–7.4 m in intervals III–XII (sets 1, 3, and 4). This increase in spacing partly reflects the stepwise decrease in fracture frequency with depth described earlier (Figure 3).

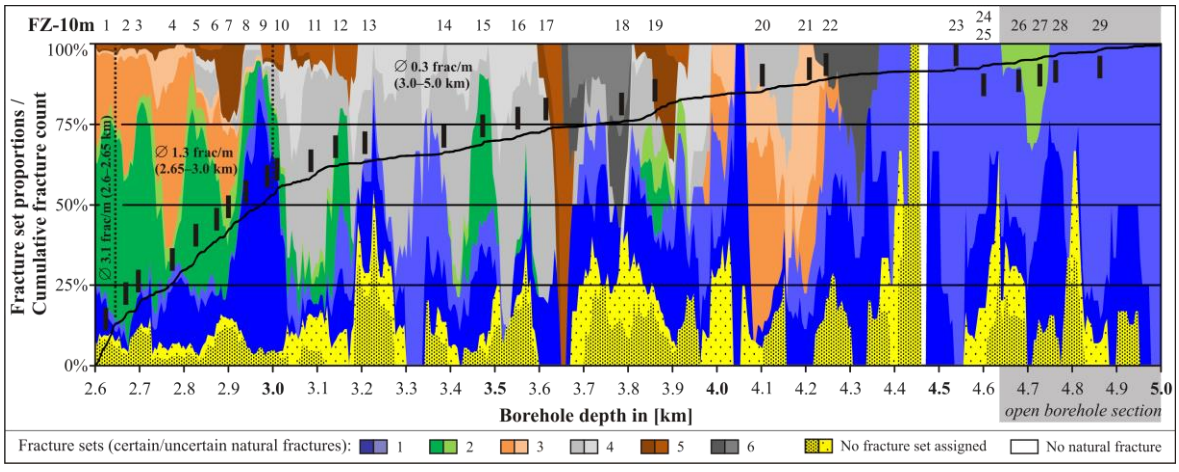

Figure 3: Fracture set disposition and cumulated fracture count versus depth. Calculation of fracture set proportions was done using a 50 m long sliding window. Zones of high fracture frequency (FZ-10m) are shown.

4.2 Comparison of Fracture Counts and Fracture Frequencies

A total of 1164 natural fractures were identified between 2600 and 5000 m, of which about 75% (N = 875) were classified as certain and 25% (N = 289) as uncertain. The proportion of uncertain fractures increases with depth from 14% at 2600–3000 m to 63% at 4600–5000 m. Figure 5 shows a comparison of results from this study with those of previous analyses. Considerable differences

in the total count of fractures are evident. The profiles of natural fracture frequency for the three datasets, derived using a 10 m bin size, show qualitative similarities, such as a high fracture frequency in the uppermost 400 m of the borehole, which most likely reflects a palaeo-weathered zone since the interface with the sediments lies at ~2507 m (Figure 1b; Section 2.2). The profile of fracture frequency for this zone obtained in this study is similar in form to that obtained by Ladner (2014, pers. comm.), but contains many more fractures. The profile of Fabbri (2011) has slightly more fractures, but they are distributed differently. Other local differences in fracture frequency between the three studies are denoted by the red frames in Figure 5 and summarised in Table 4.

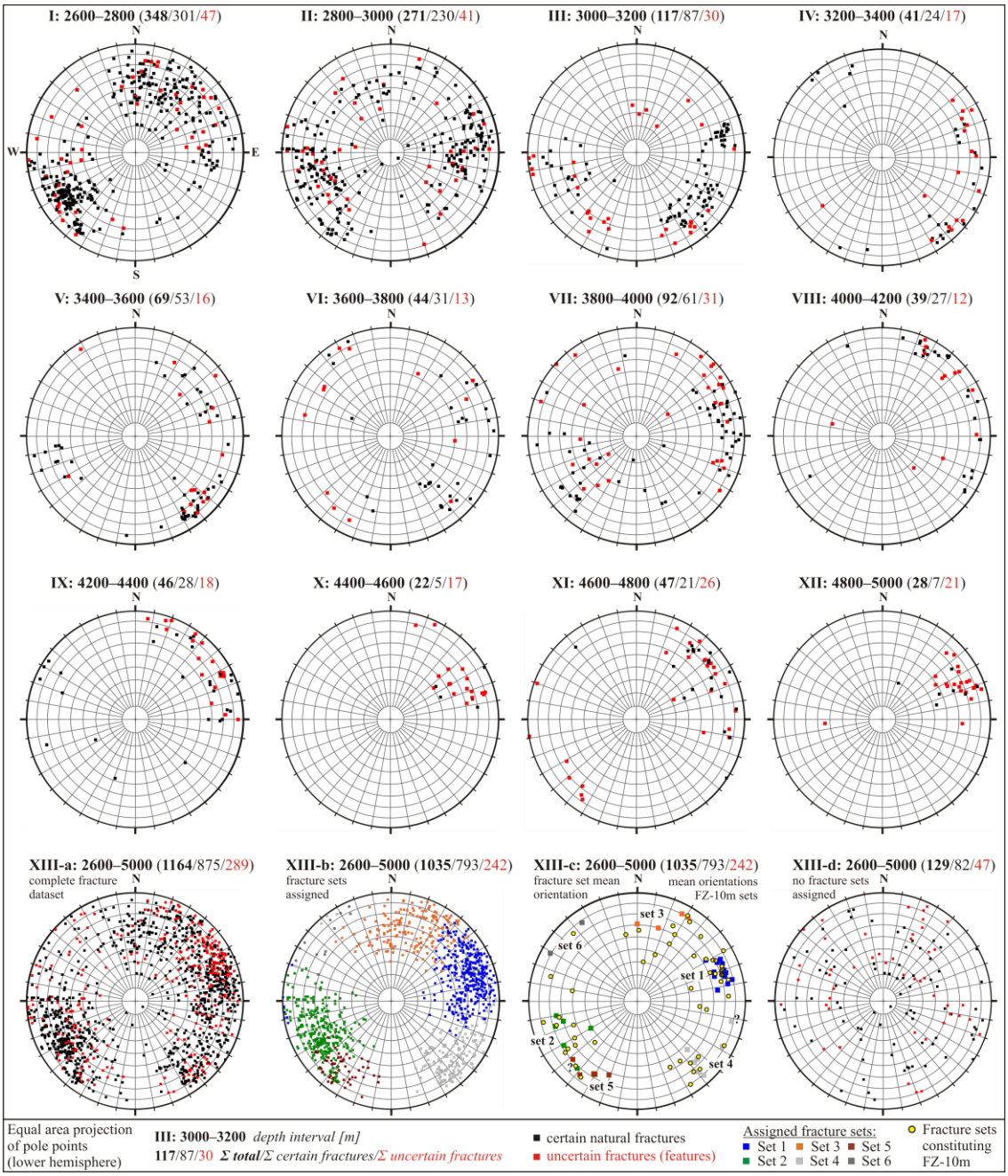

Figure 4: Equal area plots of poles to certain and potential natural fractures identified in specific depth intervals (I–XII and XIII-a). Fractures assigned to one of the six recognised fracture sets are shown as interval XIII-b. Fracture set mean orientations in 200-m-intervals and fracture sets constituting zones of high fracture frequency (FZ-10m) are shown as XIII-c (Sections 3.2.2 and 4.3, and Table 2). Fractures not assigned to any of these sets are presented as XIII-d.

4.3 Localised Zones of High Fracture Frequency (FZ)

Figure 5 shows numerous localised zones where the fracture frequency is higher than the local background. The 10 m averaging window identified 29 zones with lengths of up to 100 m, and the 2 m window gave 43 zones with lengths up to 28 m. However, below 4 km, which contains the open-hole section, the number and distribution of the zones identified with the two window lengths is almost identical. All zones identified with the 10 m window are listed in Table 5. A cluster analysis was applied to the poles of the fractures in each zone to identify sets (independent of sets 1–6 of Table 2). Most zones are formed by a dominant set, either occurring singly or with other sets, although a few zones contain two or more (similarly dominant) fracture sets (zone numbers 7, 8, 12, 15, and 19). The mean orientations of the identified sets are listed in Table 5.

Table 2: Occurrence and mean orientation of fracture clusters within 200-m-intervals (bold signifies dominant clusters; italic signifies clusters with less than 5 certain fractures; (...) denote clusters that cannot be clearly assigned to a set)

Interval		Fracture cluster orientation: dip direction/dip angle; natural fracture count (N): [certain/uncertain]						
No.	Depth [km]	**Set 1**	**Set 2**	**Set 3**	**Set 4**	**Set 5**	**Set 6**	**Rest**
I	2.6–2.8	252/64; [38/10]	**059/68; [139/15]**	196/60; [99/13]		*021/62; [4/2]*		[21/7]
II	2.8–3.0	**262/64; [85/10]**	**080/65; [77/16]**	180/61; [21/5]	314/54; [10/4]	038/75; [20/1]		[17/5]
III	3.0–3.2	259/74; [22/5]	075/60; [17/3]		**314/66; [43/7]**	*030/67; [2/7]*		[3/8]
IV	3.2–3.4	254/73; [6/8]			**318/81; [12/5]**			[6/4]
V	3.4–3.6	239/63; [11/4]	073/68; [11/1]		**319/75; [25/9]**			[6/2]
VI	3.6–3.8	**250/74; [9/2]**			317/66; [14/1]	*031/67; [2/3]*	*145/78; [3/4]*	[3/3]
VII	3.8–4.0	**246/75; [22/10]**	060/41; [6/7]		(282/78; [11/6])	(048/69; [11/1])		[11/7]
VIII	4.0–4.2	257/79; [6/2]		**211/80; [14/7]**	298/78; [5/0]			[2/3]
IX	4.2–4.4	**252/75; [12/10]**		207/80; [6/8]			119/81; [5/0]	[5/0]
X	4.4–4.6	***249/65; [4/15]***						[1/2]
XI	4.6–4.8	**243/75; [16/17]**	*(042/72; [0/5])*					[5/4]
XII	4.8–5.0	**244/71; [5/19]**						[2/2]
∑(N) = [875/289]		[236/112]	[250/47]	[140/33]	[120/32]	[39/14]	[8/4]	[82/47]

Table 3: Mean values of fracture set 'true' spacing within 200-m-intervals (bold: dominant sets)

Interval		Fracture mean spacing in [m]					
No.	Depth [km]	**Set 1**	**Set 2**	**Set 3**	**Set 4**	**Set 5**	**Set 6**
I	2.6–2.8	1.8	**0.6**	1.1		*(16.4)*	
II	2.8–3.0	**0.9**	**1.2**	2.6	6.8	2.9	
III	3.0–3.2	2.5	5.1		**1.7**	13.8	
IV	3.2–3.4	4.3			**2.4**		
V	3.4–3.6	7.0	12.2		**1.6**		
VI	3.6–3.8	**7.4**			7.8[a]	17.2[b]	13.2
VII	3.8–4.0	**2.6**	3.6[c]		(3.6)	(12.1[d])	
VIII	4.0–4.2	5.3		**2.4**	7.2[e]		
IX	4.2–4.4	**2.8**		3.7[f]			6.9[g]
X	4.4–4.6	**5.1**					
XI	4.6–4.8	**1.6**	(4.2[h])				
XII	4.8–5.0	**3.0**					

Sets occurring in a small interval: [a] 3602–3616 m, 3707–3747 m; [b] 3627–3658 m; [c] 3857–3916 m; [d] 3849–3917 m; [e] 4102–4169 m; [f] 4202–4261 m; [g] 4281–4348 m; [h] 4676-4732 m.

Table 4: Local differences in fracture frequency between this and other studies

Location No.[a]	Interval [m]	Observation with respect to the present analysis	Reference[b]
i	2600–2640	lower fracture frequency	F, L
ii	2600–3000	considerably lower amount of natural fractures	L
iii	2700–2760	considerably higher frequency of uncertain fractures	F
iv	2780–2850	considerably higher frequency of certain natural fractures	F
v	2950–3650	occurrence of almost no uncertain fractures	L
vi	3200–3450	considerably higher frequency of uncertain fractures	F
vii	3650–3670	higher natural fracture frequency of ~1.5 fractures/m	L
viii	3960–4010	higher fracture frequency	L
ix	4090–4110	higher fracture frequency of 1.2–2.5 fractures/m	F, L
x	4410–4550	higher fracture frequency	F, L
xi	4600–5000	this study: lower amount of fractures (open borehole section)	-

[a] Location number as shown in Figure 5; [b] F: Fabbri (2011); L: Ladner (2014, pers. comm.).

4.4 Localised Zones of Low P-wave Velocity (LVZ) and/or Low Bulk Density (LDZ)

Figure 6 shows profiles of density, p-wave velocity, dynamic Young's modulus, and borehole cross-sectional area from the wireline logs. For comparison, the profiles of natural fracture frequency obtained with a 5 m window for certain and uncertain factures are shown. The high fracture frequency between 2.6 km and 3.0 km clearly correlates with a low p-wave velocity and Young's modulus, but density is less affected. However, a more subtle, progressive trend towards higher density can be discerned from 2.6 km to 5.0 km, which is not obviously related to fracture frequency. We attribute this trend to lithological change with less dense and possibly weathered biotite-granites at the upper section to comparably denser monzogranites and monzonites at the lower section. The origin of the higher density between 3660 and 3710 m, and the fluctuations between 3870 and 4350 m, are not well understood, although variations in lithology and fracture frequency can be excluded.

Using the procedure described in Section 3.2.2, a total of 37 localised zones of anomalously low velocity (LVZ) and/or low bulk density (LDZ) were identified. The lengths of these zones range between 0.8 m and 31 m. Zone depth and numbering are indicated in Figure 7. Of these, 22 zones showed both low velocity and low density, 9 zones had just a low density, and 6 zones had just a low velocity. The low velocity and slightly high density which defines zone 8, is most likely caused by a lamprophyric dyke, an

interpretation supported by cuttings (Käser et al., 2007) and a negative potassium and positive thorium excursion seen in the SGR log.

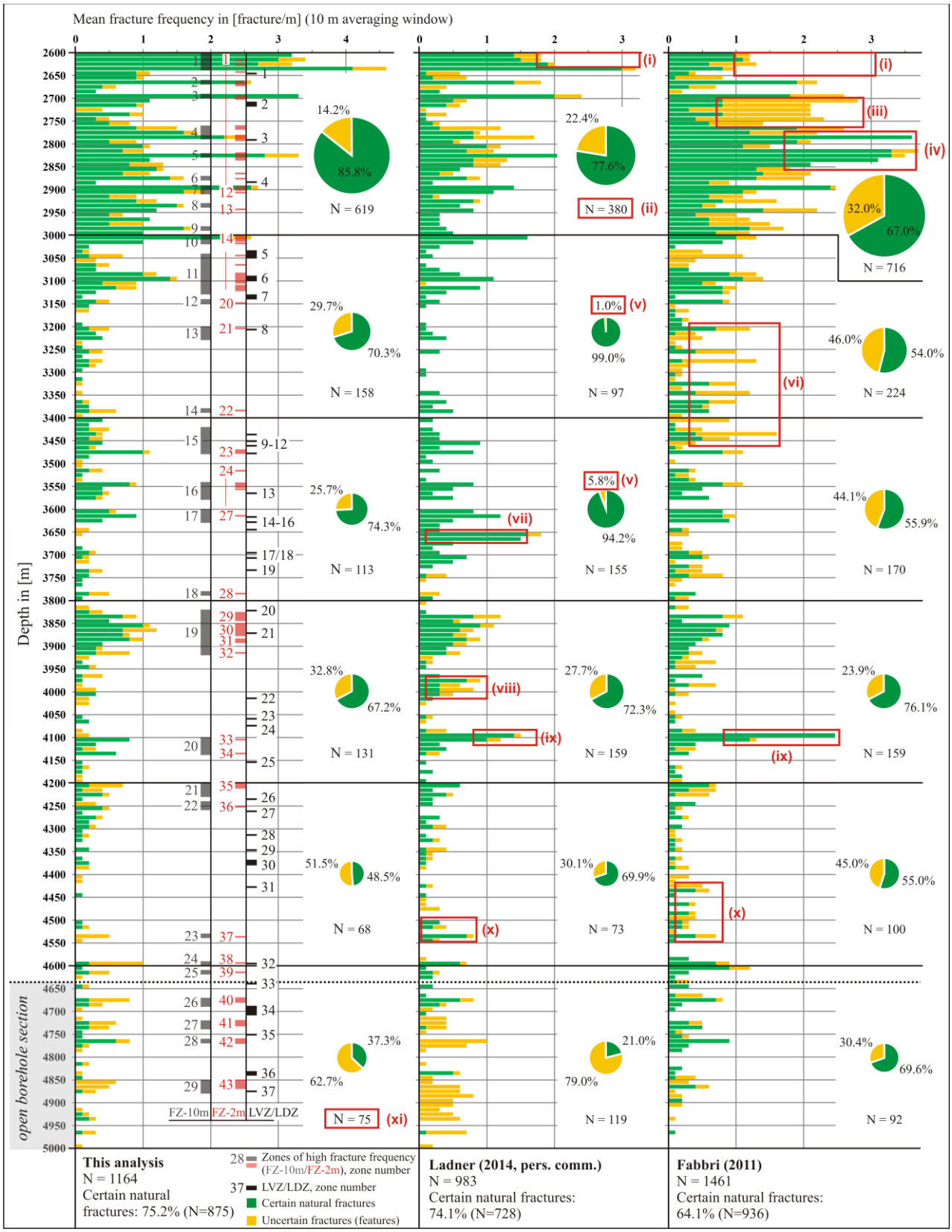

Figure 5: Comparison of fracture counts (N) in successive 400 m intervals, and fracture frequency (10 m window) from three different studies of the Basel-1 UBI log. Certain and uncertain natural fractures are shown in different colours. The red boxes indicate locations where the results of either of the two previous studies differ from the present study. Localised zones of high fracture frequency, i.e., potential fracture zones, are indicated and numbered (columns FZ-2m and FZ-10m). Zones of anomalously low velocity and/or low bulk density are shown (column LVZ/LDZ).

Table 5: Zones of high fracture frequency identified with a 10 m window (mean dip and dip direction of fracture sets that constitute each zone are given; orientations marked bold signify the dominant fracture set within a zone)

FZ-10m No.	Centre depth [m]	Length [m]	Fracture set orientation(s): dip direction/dip angle	FZ-10m No.	Centre depth [m]	Length [m]	Fracture set orientation(s): dip direction/dip angle
1	2620	40	**054/70**; 210/51; 277/55	16	3560	40	**317/75**; 210/60
2	2665	10	**206/66**; 045/45	17	3615	30	**319/65**; 248/74
3	2695	10	**055/66**; 202/38	18	3785	10	**137/74**
4	2775	30	**182/55**; 242/69	19	3870	100	257/76; 054/59
5	2825	10	**078/62**; 253/71	20	4120	40	**211/81**; 297/80
6	2875	10	**106/71**	21	4215	30	**214/77**
7	2900	20	036/76; 171/52	22	4250	20	**251/72**
8	2935	10	069/52; 250/73; 324/58	23	4535	10	**253/72**
9	2985	10	**275/49**	24	4595	10	**232/57**
10	3010	20	**257/69**; 059/56; 333/58	25	4615	10	**267/74**
11	3085	90	**312/66**; 077/77; 190/30	26	4680	20	**240/82**; 257/43
12	3145	10	249/62; 099/50	27	4730	20	**252/72**; 043/71
13	3215	30	**327/81**; 251/66	28	4765	10	**225/73**
14	3385	10	**243/71**	29	4865	30	**248/74**
15	3450	60	321/73; 073/66; 239/64				

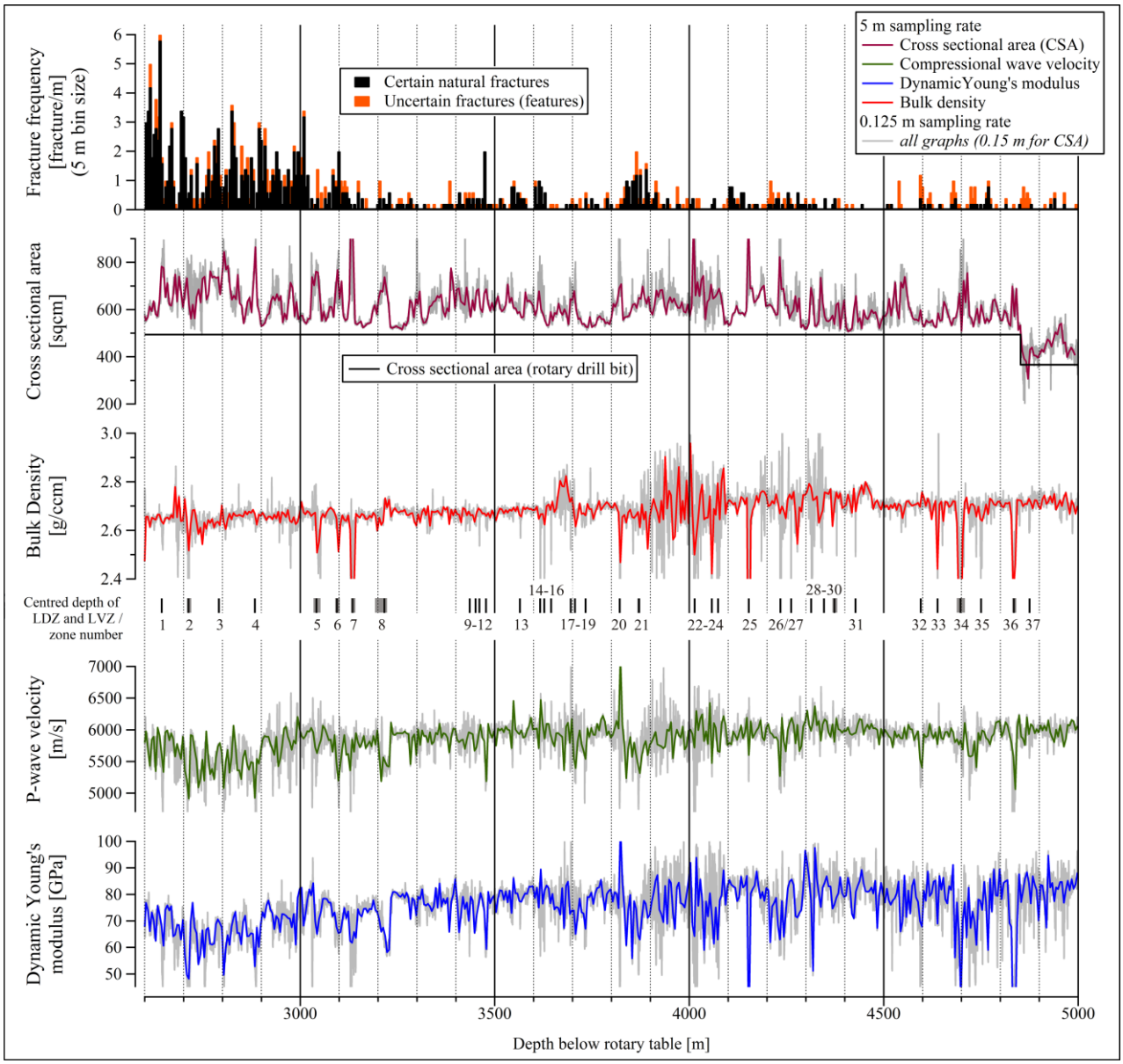

Figure 6: Overview of natural fracture frequency compared with cross sectional area, bulk density, p-wave velocity, and dynamic Young's modulus between 2600 and 5000 m. The centred depths of selected low velocity (LVZ) and low density zones (LDZ) are given (LVZ/LDZ with length > 10 m are indicated in grey).

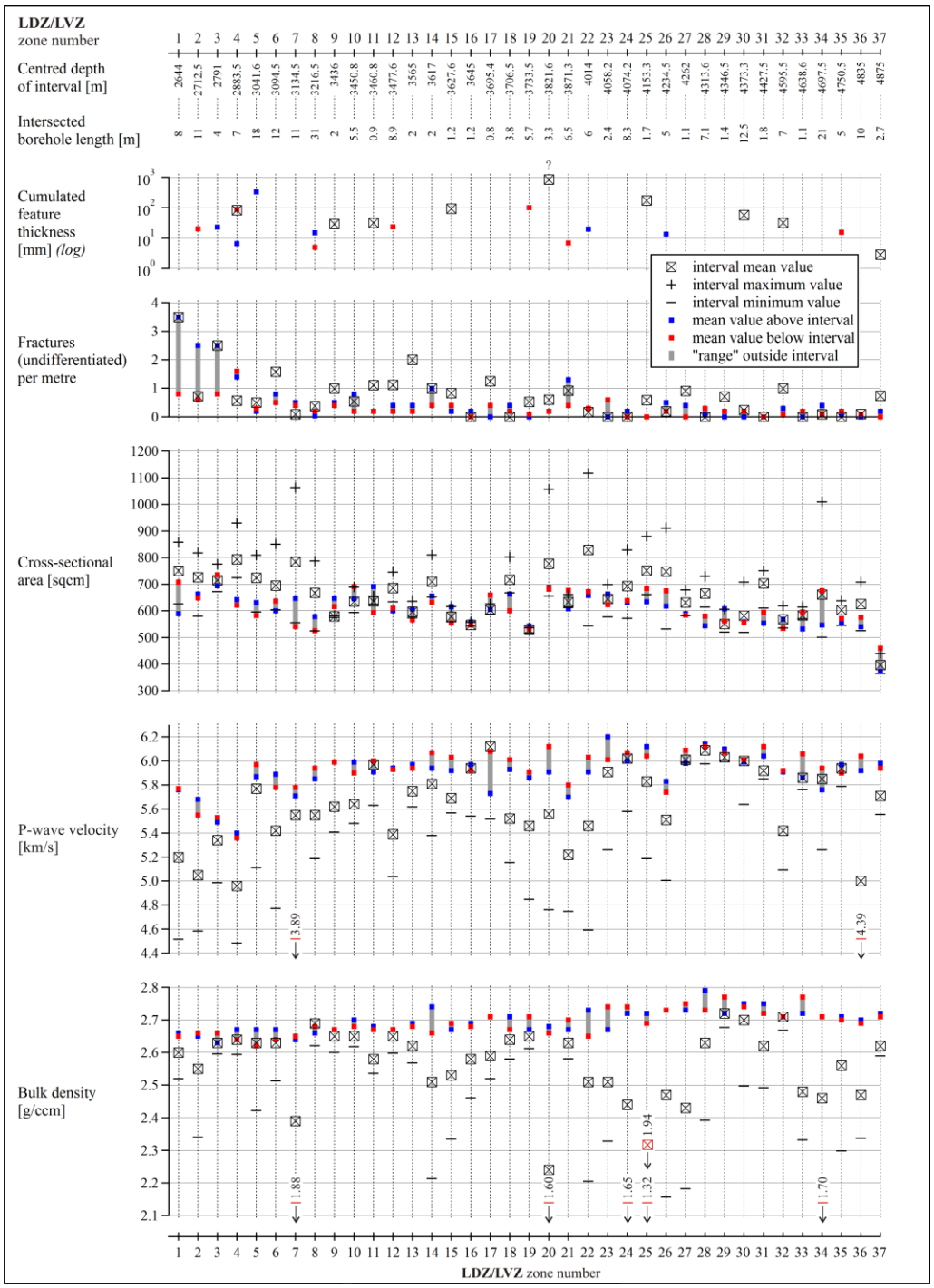

Figure 7: Comparison of bulk density, p-wave velocity, and cross-sectional area with fracture frequency of selected borehole intervals characterised by low bulk density (LDZ) and/or p-wave velocity (LVZ).

Figure 5 compares the locations of the zones of low velocity/density with the zones of high fracture frequency. The large majority of the velocity/density anomalies do not correspond to zones of high fracture frequency (FZ-2m; Figure 5). Indeed, 54% of the low velocity/density zones either contain no fractures whatsoever, or the fracture frequency does not differ from the local background. Narrow density or velocity anomalies extending less than 3 m along the hole were identified at zones 9, 11, 15, 20, 25, and 37 (Figure 7). These zones each contain a single fracture characterised by a wide (several mm to ~1 dm thick) trace visible in the acoustic reflectivity and travel time images. Such traces may indicate considerable alteration along these fractures and/or a partially open fracture. With the exception of zone 11, these zones show a negative anomaly in both ρ_b and v_P.

The 'cataclastic fracture zones' referred to in Section 2.2 are contained in zones 34 and 36. Neither of these zones corresponds to a zone of high fracture frequency, as can be seen in Figure 5. However, zone 36 coincides with a markedly different acoustic reflectivity on the UBI log that extends from 4830.2 to 4838.1 m. This is indeed most likely a cataclastic zone, since cuttings indicate cataclastic deformation of minerals, and the spectral gamma log indicates decreased concentrations of potassium, thorium, and uranium. However, the nature of zone 34 is uncertain. This zone has a low density but little change in velocity, and the borehole is locally enlarged. The borehole appears to have partially collapsed at the top of this zone during the later stimulation injection.

5. DISCUSSION

5.1 Natural Fractures and Fracture Sets

The comparison of the number of natural fractures along the Basel-1 borehole, derived independently from the three studies, showed considerable differences. Our analysis suggests that these discrepancies are mainly caused by: occasional misinterpretation of E-DITFs (e.g., red boxes vi–x in Figure 5) and DIFs of unknown origin as natural fractures (e.g., box iv); 'undersampling' of fractures, particularly in zones of high fracture frequency in the upper-hole section (e.g., box i); and misidentification of fractures in the lower borehole section due to the low-quality UBI images arising from the stick-slip movement (box xi). Our findings emphasise the importance of distinguishing artificial, drilling-induced fractures from natural fractures, and of establishing a typology to aid systematic distinction. Correction of stick-slip motion of the UBI sonde in our study led to a reduction in the number of mapped fractures in the open-hole section, and to more reliable dip angles for the natural fractures. The low fracture frequency in this section is supported by the analysis of the drill core that contained no natural fractures. However, the UBI image of the cored section showed numerous fracture traces that have the characteristics of induced fractures which strike sub-perpendicular to continuous borehole breakouts. The origin of these drilling-induced fractures (DIFs) is not well understood (cf., Section 3.1).

Structural analysis revealed a complex disposition of fracture sets along the borehole (Figure 3). Different fracture sets are dominant in different intervals. While set 1 occurs along the entire well, sets 2–6 are limited in occurrence to specific depth intervals. Our data suggest that fracture spacing increases with depth and that the lower part of the intersected rock mass, below about 4.4 km, is dominated by a single fracture set (set 1). This set, and the conjugate set 2, strike about NNW-SSE, subparallel to the "Eggian" direction. This is in contrast to the strike directions of the most prominent, first- and second-order lineaments in the area of Basel that correspond to the Rhenish system (striking NNE-SSW) (Figure 1a, Section 2.1). WSW-ENE- to W-E-striking fractures of set 3 may be associated with the "Permian" system and Permian-Carboniferous trough formation (Thury et al., 1994, and references therein). SW-dipping fractures of sets 1 and 3 are subparallel to NW-SE-striking (Hercynian) faults that have been identified in the adjacent Dinkelberg Block around Rheinfelden (Thury et al., 1994: App. 5-3; cf., SW-dipping Eggberg and Vorwald fault systems). Set 4 and 6 fractures striking about SW-NE do not yield equivalent lineaments of larger scale in the area of Basel (cf., "Wutachian" system of SW-NE strike as found in the southern Black Forest; Mazurek, 1988, and references therein). Fractures of set 5 strike in NW-SE direction and correspond to the Hercynian system. Further research is needed to better understand the causes for the obtained fracture set orientations in the Basel region.

5.2 Zones of High Fracture Frequency

The 10 m window length identified 29 zones of high fracture frequency with lengths of up to 100 m, and the 2 m window gave 43 zones with lengths up to 28 m. The identification of such zones depends upon UBI image quality and the criteria used, such as window length and fracture frequency thresholds. Nevertheless, below 4 km, the same 11 zones were identified with the two window lengths (no. 33–43 for the 2 m window in Figure 5). These zones had lengths of 6–20 m and consisted of predominantly set 1 fractures, with a few zones dominated by set 3 fractures. If it is assumed that the zones denote structures cutting the well and that the mean orientation of the members of the dominant set in a zone indicates the overall orientation of the structure, then an estimate of the local width of the structure can be derived. The resulting estimates of zone width ranged between 1 and 7 m (corrected for zone dip). Experience from surface outcrops and deep tunnels shows that fracture zone width can vary significantly over the structure, and so our estimates of zone width are at best only point estimates. Further work is needed to better understand the architecture of these zones, particularly with regard to the relation between the orientation of the structure and that of the internal fractures.

The identification of fracture zones along a well is important for the development of EGS reservoirs. In principle, such zones might be identified as zones of high fracture frequency and/or anomalies in geophysical logs aided by an investigation of drill cuttings. Our analysis showed that zones of anomalously low density or velocity did, however, not correlate well with zones of high fracture frequency, and that narrow zones of low density/velocity of less than 3 m length often contained a single fracture characterised by a thick fracture trace up to ~1 dm in the UBI image. Clearly, analysis of cuttings is an important supplement to log interpretation. Further work will include analysis of the spectral gamma log, and also relate the results to the orientation of microseismic structures active within the reservoir during the stimulation injection.

6. CONCLUSIONS

Comparison of three analyses of natural fractures derived from an acoustic televiewer (UBI) log run in granite in the Basel-1 borehole between 2.6 and 5.0 km revealed considerable differences in the distributions of natural fractures in the crystalline basement. The differences in large part reflect the difficulty in distinguishing natural from drilling-induced fractures. Poor quality images in the open-hole section below 4.7 km resulting from stick-slip motion of the sonde were radically improved by applying a novel correction method using accelerometer data. This led to fewer natural fractures in the open section than recognised in earlier studies. Fracture frequency decreases with depth from 3.1 fractures/m near the top of the log, 100 m below the weathered granite palaeo-surface, to 0.3 fractures/m below 3.0 km. Orientation cluster analyses revealed a complex pattern of up to 6 potential fracture sets along the well, some of which may be conjugate pairs. Only set 1 (steeply dipping to W–SW) is present along the entire imaged borehole, the other sets occurring over limited sections of the hole. The mean orientation of set 1 does not coincide with prominent NNE-striking Rhenish lineaments (faults) of first- and second-order in the Basel area, but strikes sub-parallel to the maximum principal horizontal stress. Fractures belonging to set 1 are spatially clustered and form localised zones of high fracture frequency. Zone lengths ranged up to 100 m, but were more typically tens of metres, and below 4 km the zones consisted predominantly of fractures belonging to set 1. Zones of high fracture frequency did not necessarily coincide with low density or p-wave velocity anomalies, as might be expected from fracture zones with damage or higher porosity. Indeed, more than half of the identified zones of low density/velocity contained no fractures or a similar fracture frequency compared to the local background. Narrow density/velocity anomalies with lengths less than 3 m were often correlated with single natural fractures characterised by several cm-thick traces in the acoustic reflectivity and travel time images, suggesting considerable alteration along these fractures and/or partially open fractures. Other zones of low density/velocity arose from lithological variations, such as lamprophyric dykes.

ACKNOWLEDGEMENTS

We thank Geo-Energy Suisse for permission to publish these data and acknowledge the support of Project GEOTHERM-2 that is jointly funded by the ETH Competence Centre for Environment and Sustainability (CCES), the ETH Competence Centre for Energy and Mobility (CCEM), and the Swiss Federal Office of Energy (BFE). We are grateful to Florentin Ladner of Geo-Energy Suisse for useful discussion.

REFERENCES

Deichmann, N., Kraft, T., and Evans, K.F.: Identification of faults activated during the stimulation of the Basel geothermal project from cluster analysis and focal mechanisms of the larger magnitude events, *Geothermics*, doi: 10.1016/j.geothermics.2014.04.001, (2014), 14 pp.

Dèzes, P., Schmid, S.M., and Ziegler, P.A.: Evolution of the European Cenozoic Rift System: interaction of the Alpine and Pyrenean orogens with their foreland lithosphere, *Tectonophysics* **389**, (2004), 1–33.

Evans, K.F., Genter, A., and Sausse, J.: Permeability creation and damage due to massive fluid injections into granite at 3.5 km at Soultz: Part 1 - Borehole observations, *J. Geophys. Res.*, **110**, doi: 10.1029/2004JB003168, (2005), 19 pp.

Fabbri, S.C.: Correlation of stress variations and natural fractures in the Basel geothermal borehole, BSc. Thesis, ETH Zurich, (2011), 39 pp.

Gürler, B., Hauber, L., and Schwander, M.: Die Geologie der Umgebung von Basel mit Hinweisen über die Nutzungsmöglichkeiten der Erdwärme, Beiträge zur geologischen Karte der Schweiz, Lieferung 160, Bern, (1987), 33 pp.

Hammah, R.E., and Curran, J.H.: Fuzzy cluster algorithm for the automatic identification of joint sets, *Int. J. Rock Mech. & Min. Sci.* **35**, (1998), 889–905.

Häring, M.O.: Technischer Bericht Geothermie-Sondierbohrung Otterbach 2, Basel, Internal Report, Geothermal Explorer Ldt., Basel, (2001), 25 pp.

Häring, M.O., Schanz, U., Ladner, F., and Dyer, B.C.: Characterisation of the Basel 1 enhanced geothermal system, *Geothermics* **37**, (2008), 469–495.

Heitzmann, P.: Kakirite, Kataklasite, Mylonite – Zur Nomenklatur der Metamorphite mit Verformungsgefügen, *Eclogae geol. Helv.* **78**, (1985), 273–286.

Hinsken, S., Ustaszewski, K., and Wetzel, A.: Graben width controlling syn-rift sedimentation: the Palaeogene southern Upper Rhine Graben as an example, *Int. J. Earth Sci.* **96**, (2007), 979–1002.

Käser, B., Kalt, A., and Borel, J.: The crystalline basement drilled at the Basel-1 geothermal site. A preliminary petrological-geochemical study. Institut de Géologie et d'Hydrogéologie, Université de Neuchâtel. Internal report, (2007), 45 pp.

Ladner, F., Schanz, U., Häring, M. O.: Deep-Heat-Mining-Projekt Basel: erste Erkenntnisse bei der Entwicklung eines Enhanced Geothermal System (EGS). *Bull. angew. Geol.* **13**, (2008), 41–54.

Laubscher, H.: Plate interactions at the southern end of the Rhine graben, *Tectonophysics* **343**, (2001), 1–19.

Mazurek, M.: Geology of the crystalline basement of northern Switzerland and derivation of geological input data for safety assessment models. Technical Report, 93-12, Nagra, Wettingen (Switzerland), (1998), 236 pp.

Meyer, J.: Die Kataklase im kristallinen Untergrund der Nordschweiz, *Eclogae Geol. Helv.* **80**, (1987), 323–334.

Priest, S.D.: Discontinuity analysis for rock engineering, Chapman & Hall, London, (1993), 473 pp.

Schmitt, D.R., Currie, C.A., and Zhang, L.: Crustal stress determination from boreholes and rock cores: Fundamental principles, *Tectonophysics* **580**, (2012), 1–26.

Sikaneta, S., and Evans, K.F.: Stress heterogeneity and natural fractures in the Basel EGS granite reservoir inferred from an acoustic televiewer log of the Basel-1 well, *Proceedings*, 37th Workshop on Geothermal Reservoir Engineering, Stanford University, Stanford, CA, (2012), 12 pp.

Terzaghi, R.D.: Sources of error in joint surveys, *Geotechnique* **15**, (1965), 287–304.

Thury, M., Gautschi, A., Mazurek, M., Müller, W.H., Naef, H., Pearson, F.J., Vomvoris, S., and Wilson, W.: Geology and hydrogeology of the crystalline basement of northern Switzerland. Synthesis of regional investigations 1981–1993 within the Nagra Radioactive Waste Disposal Programme, Technical Report, 93-01, Nagra, Wettingen (Switzerland), (1994), 471 pp.

Ustaszewski, K.: Reactivation of pre-existing crustal discontinuities: the southern Upper Rhine Graben and the northern Jura Mountains – a natural laboratory, Ph.D. Thesis, University of Basel, (2004), 145 pp.

Ustaszewski, K., and Schmid, S.M.: Latest Pliocene to recent thick-skinned tectonics at the Upper Rhine Graben - Jura Mountains junction, *Swiss J. Geosci.* **100**, (2007), 293–312.

Valley, B.: The relation between natural fracturing and stress heterogeneities in deep-seated crystalline rocks at Soultz-sous-Forêts (France), Ph.D. Thesis, ETH Zurich, (2007), 245 pp.

Valley, B., and Evans, K.F.: Stress orientation to 5 km depth in the basement below Basel (Switzerland) from borehole failure analysis, *Swiss J. Geosci.* **102**, (2009), 467–480.

Ziegler, P.A.: European Cenozoic rift system, *Tectonophysics* **208**, (1992), 91–111.